Int J Adv Manuf Technol (2016) 82:99–109
DOI 10.1007/s00170-015-7334-5

ORIGINAL ARTICLE

Study on microstructures and mechanical properties of super narrow gap joints of thick and high strength aluminum alloy plates welded by fiber laser

Z. H. Zhang [1,2,3] · S. Y. Dong [2] · Y. J. Wang [2] · B. S. Xu [1,2] · J. X. Fang [1,2] · P. He [1]

Received: 9 January 2015 / Accepted: 18 May 2015 / Published online: 4 June 2015

Abstract The welding of thick high strength aluminum alloy plate was exceedingly difficult. Traditional arc welding was prone to softening the welded joints and involves multilayer; meanwhile, multi-pass welding may cause great residual welding stress, and deformation resulted in dampening the wide expansion of the welding structure of thick high strength aluminum alloy plates. Therefore, it was urgent to develop advanced materials and welding technologies to enhance the comprehensive mechanical properties of welded joints. Fiber laser boasted the advantages such as perfect monochromaticity and high quality light beam. In order to decrease the thermal loss of the welding heat source on the matrix, small power fiber laser and super narrow gap groove were applied for the effective welding of the 20-mm thick 7A52 aluminum alloy. The welding adopted multilayer and single pass welding with the groove width no wider than 4 mm. The weld was composed of four layers and the size was no wider than 4.5 mm, which was basically consistent with the widths of the whole. The parent metal was welded with 5183 alloy and 5E06 alloy. Fiber optical microscope, scanning electron microscope (SEM), transmission electron microscope (TEM), and tensile testing machine were employed to investigate the influence of Er-Zr microalloying aluminum alloy welding wires upon the microstructure and mechanical properties of the welded joints.

Keywords 7A52 aluminum alloy · Super narrow gap groove · 5E06 alloy · Joint microstructures · Mechanical properties

✉ P. He
576492531@qq.com

[1] State Key Laboratory of Advanced Welding and Joining, Harbin Institute of Technology, Harbin 150001, China

[2] National Key Laboratory for Remanufacturing, Academy of Armored Forces Engineering, Beijing 100072, China

[3] Department of Mechanical Engineering, Academy of Armored Force Technology, Changchun, Jilin 130117, China

1 Introduction

High strength aluminum alloy generally refers to the aluminum alloy whose tensile strength is more than 480 MPa, chiefly the 7XXX series. Such modern industries as aerospace aviation, shipbuilding, and military equipment manufacturing are having increasing demands for aluminum alloy components featuring perfect toughness and corrosion resistance. Therefore, low density and high specific strength thick aluminum alloy plates with moderate thickness compose the critical structural materials of a high usage level and processing technology in national economy, national defense, and military industry. For the time being, 70–80 % high strength aluminum alloy has been applied in civil aircraft and 40–60 % in military aircraft. Traditionally, the aluminum alloy is riveted, which could increase the weight of the structure, and welding is the first choice in solving this problem. Nonetheless, due to the high oxidizability, thermal conductivity and specific heat capacity of the aluminum alloy and the massive cracking tendency, easy formation of cavities and slag inclusion of the welded joints, highly effective new welding technology, and material systems needs prompt development [1]. Traditionally, the welding of thick aluminum alloy plates applies technologies such as gas shielded welding technology and submerged arc welding technology, which have the disadvantages of numerous weld passes, preheating, numerous difficulties in adjustment after welding, low productivity, and severe

softening in the heat affected zone (HAZ) due to great heat input of arc welding in the process of high strength aluminum alloy welding [2–4]. For this reason, thick and high strength plate welding technology mainly focuses on enhancing the welding efficiency, improving the quality of products, and reducing the cost of production. The welding methods are selected on the principle of increasing the depth of fusion, simplifying the welding sequence, adding heat input, and reducing the sectional area of the joints.

Friction stir welding achieves favorable welding results for the welding of 2XXX and 7XXX aluminum alloy series and that of different thicknesses, but the disadvantages such as large upsetting force, high tooling requirements, difficulties in three-dimensional flexible processing, and low welding speed have impeded the engineering application of aluminum alloy [5–9]. With the incomparable superiorities of in single pass weldable thickness, the electron beam welding may hit a (EBW) penetration depth of 300 mm. However, it can only be carried out in the vacuum environment, and as the size of the vacuum chamber is usually not big enough, this approach cannot be adopted in the welding of large-sized work pieces, thus blocking wits application in the industrial areas [10]. Laser welding becomes an approach suitable for aluminum alloy welding due to the penetration fusion cavities that endow laser welding with high energy density, rapid heating, and cooling in addition to the possibility to gain narrow weld. Laser welding can be used for complicated flexible three-dimensional processing, and is easy to realize automation and boasting extensive prospects for commercial application [11]. With the evolution of high-power high quality fiber laser and the development of the compound welding technology of laser arc welding, the thickness of weldable aluminum alloy can be remarkably increased. When high-power laser welding is applied on thick plate, the surface of materials must go through preprocessing and strict restriction of fit-up gap whose standard is exceedingly hard to control. Besides, when the heat input volume is increased, the strength and tenacity of welded joints will be declined. Since no appropriate welding wire is applied to supplement the burning losses of the alloying elements such as Mg and Zn, the defects such as solidification cracks are easy to happen to the welded joints [12, 13]; thick large power laser welding plates, due to its high heat source density, forms great temperature gradient in the weld and the narrow zone nearby, which finally generates residual stress of great gradient and uneven structural properties of welded joints, as well as negative impact on their overall mechanical properties. On the other hand, thick aluminum alloy plates welded by compound laser arc boast conspicuous advantages. However, the combination of two heat sources is bound to increase heat input volume and inappropriate control will give rise to the softening of the welded joints. As a result, it is not the best technology to weld thick and high strength aluminum alloy plates.

The present work adopts the small power laser welding technology with filler wires which can decrease the thermal losses of the joints in a better measure. Meanwhile, in combination with the advantage of super narrow gap groove, super narrow gap welding further diminishes the size of grooves based on narrow gap welding grooves. The small angle grooves can reduce the amount of filler wires, which is beneficial for the fusion of side walls. The cooling speed of thick plates is fairly high. When multilayer and single pass welding is applied, the weld layer is very thin, so that the original heat processing of the former layer welded by the latter layer is more complete. In this case, the grains of the weld metal are finer, and the sizes of the weld are smaller. The cooling speed is accelerated and the mechanical properties of welded joints are heightened [14, 15]. When rare earth elements are added into the aluminum alloy, the impurities of the alloy can be purified, the microstructures can be refined and ameliorated, and the re-crystallization will be inhibited. The function of Sc in aluminum alloy has captured wide attention of the academic circles [16–20]. Nonetheless, the high price of Sc stops the new materials of rare earth aluminum alloy from being applied outside of the laboratory. Large quantities of researches made in this year indicate that Er and Zr have similar functions with Sc in aluminum alloy except for their low costs [21–24].

Superior welding technology can influence the advance of materials, and perfect weld groove design in addition to welding material optimization can reinforce the overall mechanical properties of welded joints. The objective of this work was to present laser welding of aluminum alloys using fiber laser with perfect weld groove design and micro-alloying Al-Mg-Mn alloy welding wire. This paper selects fiber laser in combination with super narrow gap groove to weld the 20 mm 7A52 aluminum alloy plates with filler wires. The welding wire is made of 5183 alloy and Al-Mg-Mn alloy compound with Er and Zr. The measures of microscopic analysis and property testing are adopted to make a comparative analysis of the impact of different welding materials upon the microstructures and mechanical properties of the welded joints and analyze the mechanism of the microstructures and properties of the joints of thick 7A52 aluminum alloy plates welded by super narrow gap laser optimized by welding wire of 5E06 alloy.

2 Experimental procedures

The parent metal for the experiment is the rolled 7A52 aluminum alloy plates with a size of 160 mm×80 mm×20 mm; 5183 alloy welding wires and 5E06 alloy welding wires are employed, whose diameters are both 1.6 mm. The composition of the parent metal and the two kinds welding wires are listed in Table 1. The welding experiment applies fiber laser produced by IPG whose maximum rated power output is

Table 1 Chemical composition of 7A52 and 5183 and 5E06 (wt.%)

Alloy	Zn	Mg	Cu	Mn	Cr	Ti	Zr	Er	Fe	Si	Al
7A52	4.2	2.1	0.08	0.30	0.16	0.08	0.14	–	≤0.30	≤0.25	Bal.
5183	–	4.7	–	0.8	–	0.1	–	–	–	–	Bal.
5E06	–	4.9	–	0.7	–	–	0.1	0.3	–	–	Bal.

4000 W and the wave length is 1.06 μm. Two-dimensional welding machine is used as the motor execution system. The welded joints are butted, and the schematic diagram of welding groove is illustrated in Fig. 1, in which single U and I grooves are adopted together. False boss is left at the bottom of the weld, which will be removed by machining after welding.

Clean the parent metal in the welding zone before the welding with 30 % NaOH solution first and then by 30 % HNO_3 solution. The materials are dried and preserved after water washing. Scrub the materials with acetone before the welding. The pre-welding period should not be longer than 8 h. To protect the focus lens from the pollution of reflection laser, the laser head should be leaned at a 10-degree angle towards the direction of welding, that is, the direction of plate rolling. Figure 2 is the schematic diagram of the welding process. Firstly, pure laser is applied for penetration fusion welding at the bottom of the groove. For the sake of complete penetration of false boss, the laser focuses at 1 mm below the plate surface. Laser welding with filler wire is applied from the second pass welding to the cosmetic welding. A pass welding follows the previous one after the groove is cleaned. Four passes are wielded altogether with the interlayer temperature uncontrolled, and each welding is done after the temperature of the plate is naturally cooled to the room temperature. The technical parameters of the welding are given in Table 2. Under the effects of horizontal constriction during the welding, the groove width of 4 mm at the ladder will shrink to 3 mm or so. In order to ensure perfect fusion of side walls and interlayers, the diameter of laser spot is set to 3 mm, which is the equal size of the groove. Special guide wire nozzle is made to feed the filler wire to the laser spot with the angle between the welding wire, and the horizontal plane is maintained at 60°. Thick plates are linked in the multilayer and single pass manner from the bottom up. The front of the weld is safeguarded by shielding gas. The protective gas is mixed by 50 % He+50 % Ar. Pure Ar is applied in the notch of the clamp to prevent the false boss bath from excessive penetration, and certain pressure is added to the back of the bath for compulsive shaping of the weld.

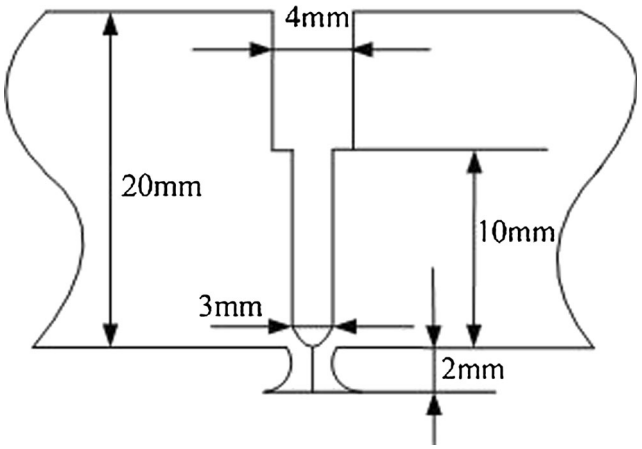

Fig. 1 Groove diagram for welding

The metallographic specimen of the section of weld vertical to the weld is cut out for analyzing the microstructure of the joint. The metallographic specimens go through metallographic polishing, burnishing, and sampling first and then erosion by Keller's reagent for about 30 s. Observation and analysis of the metallographic microstructures are carried out under the PMG3 metallographic microscope, and then Philips Quant 200 scanning electron microscope is adopted to observe the morphology of fracture of the welded joints. The hardness of the welded joint is tested on the HVS-1000 digital microhardness tester. Hardness test is carried out, for 10 s, respectively, for the surface and bottom transverse sections of the joint and the vertical weld welded by two sorts of different welding wires, with the load of 100 g. Each test is conducted on both sides at an interval of 1 mm in the middle of the transverse section of the weld from its center, and the value of hardness tested is the average of the three measurements. The same process can be carried out vertically for the value of hardness of different welding materials from 2 mm of the lower surface to the center of the upper surface. The average value is calculated from the three measurements. WE-100 universal material tester is used for tensile test at a rate of 2 mm/min to measure the tenacity of welded joints of parent metal and different welding materials. The specimens for the tensile test go through stratified sampling so that the width of the whole weld is covered in the test zone. Three parallel specimens appear in each processing state, whose average value of measurement is taken as the test value in the state. The size of tensile specimen is shown in Fig. 3 where the surface of the specimens is polished.

3 Results and discussion

3.1 Analysis of microstructures of welded joints

Figure 4 shows the process of laser welding. Due to the strong tendency of thermal expansion of aluminum alloy, rigid fixation is adopted by the device in the figure to prevent the wire

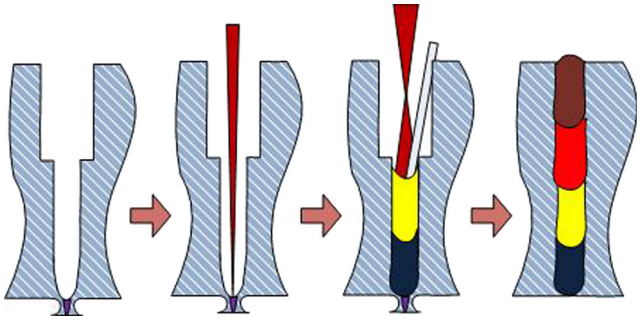

Fig. 2 Schematic diagram of the welding process

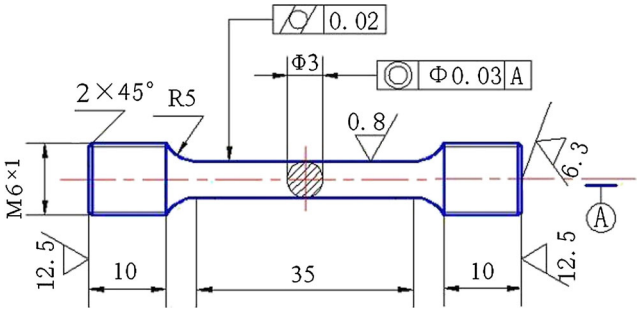

Fig. 3 Schematic diagram of standard sample

feeding nozzle from being blocked in the groove since the weld constriction during the welding may interrupt the welding. Two diverse aluminum alloy welding wires are used, where the welded joints are sound shaped. After the welding, false boss and joints welded by deep laser penetration welding are removed, only reserving the joints welded by laser with filler wires, which guarantees the entire homogeneity of the microstructures and mechanical properties of the welded joints. Since the parent metal is 7XXX aluminum alloy, the strength of welding wire should be inferior to that of the parent metal, which means it is the low matching joint [25]. For the low matching weld, narrow grooves should be applied as much as possible, and the horizontal width which is no bigger than 4 mm could relieve the strain concentration of the weld effectually. Besides, reducing the width of weld can boost the plastic flow stress. Single U and I grooves are favorable for the perfect fusion of the bottom and the side walls, and at the same time, good penetration ratio and homogeneity of composition contribute to the overall mechanical properties of welded joints [26, 27].

Figure 5 shows the local structural morphology of the transverse section of narrow gap multilayer and single pass welded joints. The interlayer and side walls are in good fusion without any failure of the fusion of interlayer and side walls, or any visible cavities, cracks or slags, etc. D. Dittrich [28] et al. adopted fiber laser in combination with super narrow gap grooves for reliable connection of thick aluminum alloy plates and applied small light spot fiber laser for the scanning and fusion of welding wires in the circular path. Nevertheless, they discovered a great number of cavities in the welded joints which seriously affected the mechanical properties of the welded joints. The cavities of the joints welded by laser were formed for complicated reasons [29]. Katayama [30] found out that the evaporation of metal steam, the introduction of protective gas, and the unstable welding would all trigger cavities. When welding wires were molten by the small light spot in the circular path, the metal flow behavior of the bath became more complex and easier to draw in gas and form cavities. The experiment made it clear that single U grooves for circular arc transition at the bottom could better solve the problem of unsuccessful fusion; defocus light spot laser heat conductance welding of equal width of gap could develop a good fusion of side walls, and laser reflection formed by curved surface of fusion and side walls became the main reason for fusion of side walls; during the welding process, the relatively fixed position of laser and welding wire enhanced the stability of the bath, which significantly avoided the formation of cavities and other defects.

Figure 6a indicates the microstructural morphology near the fusion line of welded joint filled with 5183 alloy welding wire. Figure 6b is the microstructure near the fusion line of welded joint filled with 5E06 alloy welding wire. The welded joints of two different welding materials all have the fusion zone, the HAZ, and the base material. Equiaxial structure exists in the center of the weld and the weld, zone approaches the fusion line. Some coarse columnar crystal microstructures grow in the direction of the temperature gradient. The leading edge grains extend to the weld center and form epitaxial solidification. The typical features of HAZ are the re-

Table 2 Laser welding parameters

Pass	Laser power (kW)	V_w (m/min)	V_F (m/min)
1	2000	0.6	–
2–4	3200	0.6	15

Fig. 4 Photograph of the welding process

Fig. 5 Local microstructural morphology of welded joints

crystallization of most microstructures in the processing state, and coarse re-crystallization microstructures occur in some parts. The parent metal is the microstructure without re-crystallization in the rolling state of fibriform with the grains elongated to the direction of rolling. A huge number of black dots which are the second phase precipitates distribute on the aluminum matrix. The comparison reveals that the weld of the welded joint of 5E06 alloy welding wire is primarily composed of equiaxial structure, fine grains, a few coarse columnar crystal, and equiaxed grains near the fusion line, which is narrower than the HAZ of the welded joint filled with 5183 alloy welding wire, where re-crystallization is strikingly inhibited.

Figure 7 indicates the interlayer microstructures of the weld zone where obvious interfacial transition region exists between the weld passes. The grains near the fusion line grow and the coarse grain zone and fine grain zone coexist between the layers. The reason for this is that the preceding pass will go through the process of re-fusion and thermal treatment when the latter pass is welded; the closer they are to the fusion line under the effects of laser heat the more obviously the grains grow; the direction where the grains grow in the re-fusion zone shifts; with heat dissipation of the multilayer weld bath, the direction of temperature gradient and grain growth also change. The comparison reveals that the grain zone for 5E06 alloy welding wire is narrower than that for 5183 alloy welding wire. Figure 7c and d presents the results of high power microscopic observations of the microstructures of interlayer coarse grain zone, where the coarse grain zone filled with 5183 alloy welding wires is in epitaxial solidification. However, the coarse columnar equiaxed grain generates the segregation of both the chemical composition and impurities in the weld center that declines the mechanical properties of weld metal [31], which remarkably changes the microstructures of coarse grain zone in the weld filled with rare earth micro-alloy and significantly hinders the growth of columnar grains. The reason is, as it is analyzed, that a special nucleus of heterogeneous nucleation in the welding bath destroys the pattern of epitaxial solidification. Figure 7e and f shows the microstructure in the interlayer fine grain zone in the weld center where a good amount of fine equiaxed grains and columnar grains take shape. Therefore, there are two reasons for this phenomenon. On the one hand, super narrow gap fusion bath is too small and the degree of supercooling of laser welding is very high while the latter is the critical factor in deciding the formation of equiaxed grains [32, 33]. The thermal effects of the latter layer upon the preceding layer are equivalent to short-time thermal treatment in which the preceding layer goes through twice re-crystallization during the process of heating and cooling that the grains far away from the interlayer fusion line are notably refined. For this reason, this zone has higher overall mechanical properties. On the other hand, after the welding wires are added, the flow of fusion bath is accelerated so that the microstructure of weld becomes finer and more even. H.Y. [34] discovered that fine Er-rich or Zr-rich second phase particle could stimulate the formation of equiaxed grains as the nucleus of heterogeneous nucleation. Compared with the welds of 5183 alloy welding wires, the sizes of axial dendrite in the fine-grained region filled with micro-alloyed welding wires are smaller and the amount of equiaxed grain was bigger locally.

To further identify the features of the fine grain zone, the backscattered-electron diffraction (EBSD) approach is adopted to measure the grain size in the zone. Figure 8

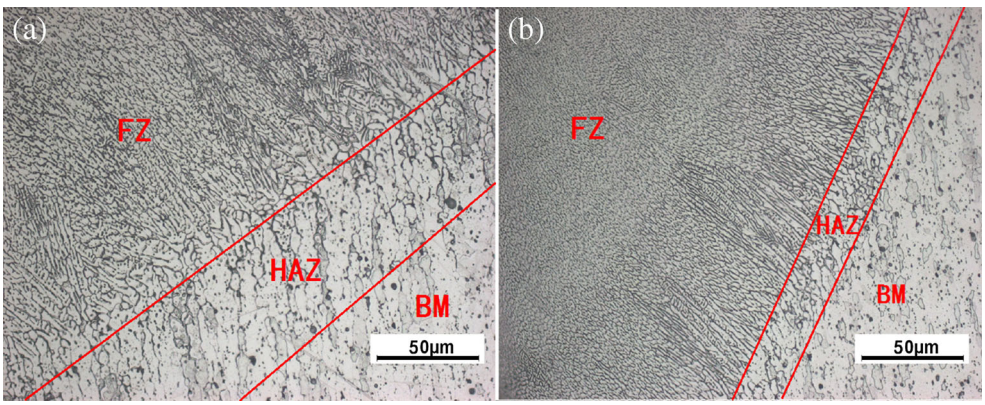

Fig. 6 **a** Microstructure near the fusion line of welded joint of 5183 alloy welding wire. **b** Microstructure near the fusion line of welded joint of 5E06 alloy welding wire

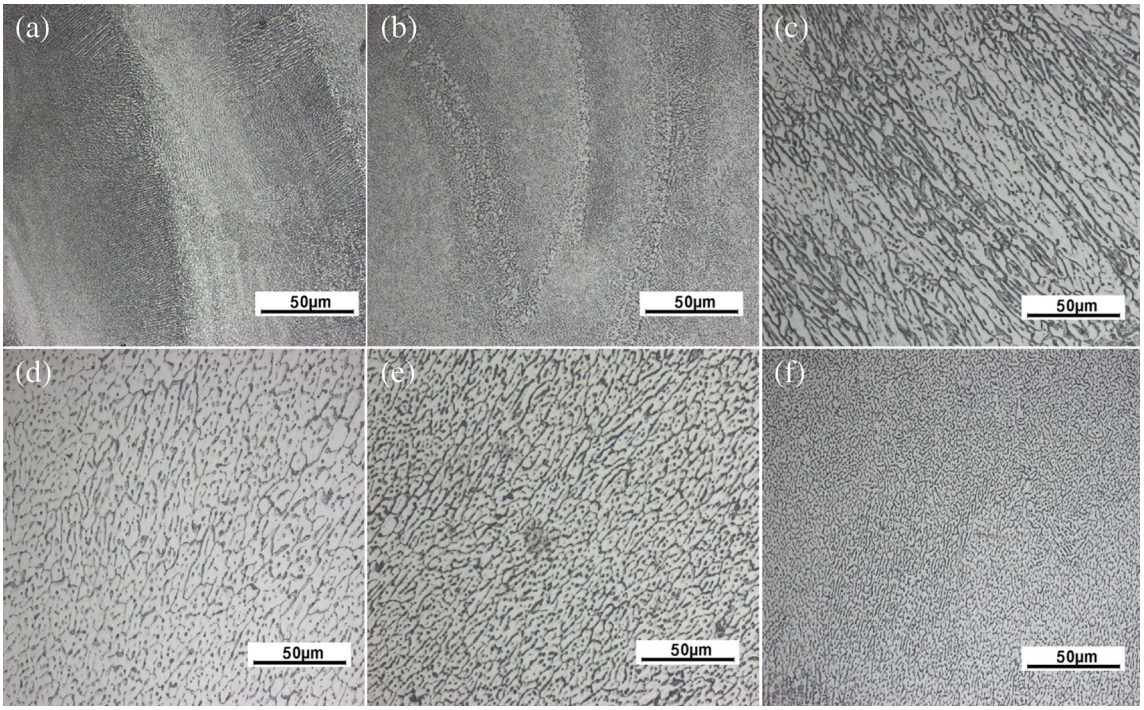

Fig. 7 **a** Interlayer microstructure in the 5183 alloy weld zone. **b** Interlayer microstructure of 5E06 alloy weld zone. **c** Interlayer coarse grain zone in the 5183 alloy weld zone. **d** Interlayer coarse zone in the 5E06 alloy weld zone **e** Interlayer fine grain zone in the 5183 alloy weld zone. **f** Interlayer fine grain zone in the 5E06 alloy weld zone

describes the morphology of grain in the fine grain zone in the weld zone where the form of organization in the center of the weld is consistent with what is observed in the metallographic phase. It is the hybrid organization of equiaxed grain and columnar crystal while a huge amount of equiaxed grains of good mechanical properties are formed in the fine grain zone stuffed with 5E06 alloy welding wire. The measurement tells that the grain size of weld filled with 5183 alloy welding wire averages out to be 168 μm, and the average grain size of the weld filled with rare earth micro-alloyed welding wires drastically diminishes to 30 μm. The process of crystallization is represented chiefly by the growth velocity of crystal nucleus and linear velocity of crystal grown from crystal nucleus. The grain size depends on the relative growth rates of crystal nucleus and grains, respectively. With the addition of metaphoric element Zr and rare element Er into the aluminum alloy welding wire, nanoscale second phase Al_3Er and Al_3 (Zr, Er) particles disperse and distribute inside the original grains of the welding wires. Because of their coherent interface with the Al matrix, the degree of lattice mismatching with Al lower than 5 % and high thermal stability, they can become the nucleus of heterogeneous nucleation of α(Al) so as to promote grain nucleation and make the weld grain size relatively finer.

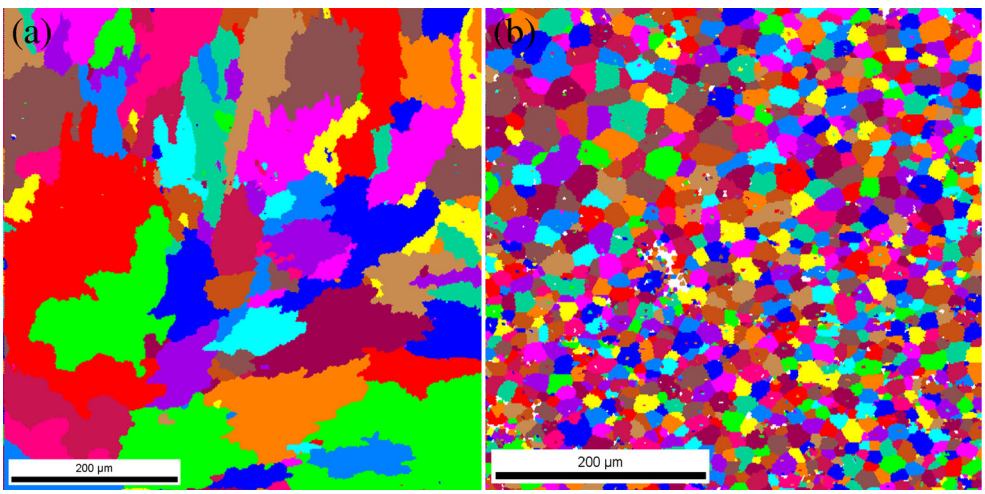

Fig. 8 EBSD image of grains in the weld zone. **a** Morphology of grains in the center of the 5183 alloy weld zone. **b** Morphology of grains in the center of 5E06 alloy weld zone

Figure 9 further observes the refined structure of the weld filled with 5E06 alloy welding wire by means of TEM. Some dislocation lines intertwine in the weld zone. Fine second phase particles appear near the dislocation area occasionally and distribute around the dislocation line and could restrain dislocation and grain boundary movement. Figure 10 presents the high angle annular dark-field imaging of the precipitated phases. Figure 10 shows the results that are manifested by EDS precipitated phase; the precipitated phase grains contain Al, Mg, and Er. To take literature [35] into consideration, it is judged that they are Al_3Er phase particles which have perfect pinning effects upon the dislocation and sub-grain boundary and play the functions of precipitation strengthening and recrystallization impediment. Meanwhile, the mismatching degree of Al_3Er and aluminum matrix is fairly low, which conforms to the size and structural conditions of the nucleus of heterogeneous nucleation [36]. When crystallization occurs, the Al_3Er phase particles and grains of matrix can be perfectly moistened to reduce the surface tension to contact the crystal surface, which is beneficial for heterogeneous nucleation to refine the grains. Figure 10c depicts the observations of another sort of particle of equal size to Al_3Er. It is judged to be the Al_3 (Er, Zr) particle which also has a good coherent relationship with the matrix. Because of the fairly high thermal stability of these particles, they can be preserved at the boundary of the bath as the nucleus of the heterogeneous nucleation to accelerate the formation of equiaxed grain [34, 36].

3.2 Mechanical properties of welded joints

3.2.1 Microscopic hardness testing

Figure 11 describes the distribution of the microhardness of surface layer and bottom layer of the transverse section of welded joints filled with different welding materials. A represents 5183 alloy welding wire and B indicates 5E06 alloy filler wire. During multilayer welding, the weld of each layer is heated again when the subsequent layer is welded, which exercises pivotal impact on the mechanical properties of welded joints. The microhardness of welded joints of two diverse filler wires is, respectively, measured from the weld center including the weld zone, the HAZ, and the parent metal zone.

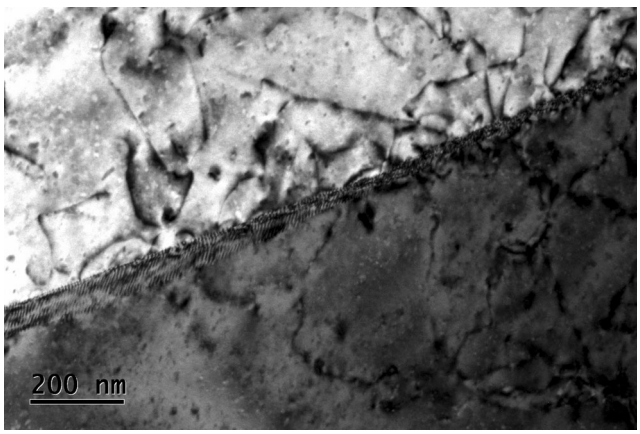

Fig. 9 TEM image of the central structure of the 5E06 alloy weld zone

The comprehensive testing results reflect that the microhardness of the weld zone of welded joints filled with two different sorts of aluminum alloy welding wires is lower than that of the parent metal. The closer it approaches the weld center, the lower the hardness is; the closer it is to the fusion line, the higher the hardness is. This is because the energy of fiber laser light spot applied is in Gaussian distribution where the energy of the spot center is most concentrated. In this case, the element Mg in the aluminum alloy welding wire is easier to produce burning losses which will lead to shrunken hardness and bring down the mechanical properties in the weld zone [37]. The hardness value rapidly rises from the weld zone to the parent metal where it tends to be stable and hits the peak in the HAZ. The abrupt rise of microhardness in HAZ is primarily because that the optimal aging temperature is obtained in this region and an aging peak zone is formed under the effects of weld thermal cycle [38]. The second reason is that the precipitated phase is re-dissolved to the matrix in the HAZ and generates the effects of solution strengthening.

The hardness of bottom layer weld zone of the welded joints filled with 5183 alloy welding wire is higher than that of the surface layer, close to that of the HAZ of the surface layer weld. This is because the bottom layer weld is influenced by the effects of thermal treatment of latter pass weld and different microstructures are formed due to grain refinement. The microhardness of welded joints filled with 5E06 alloy welding wires displays distinctive features. The microhardness of each region of the welded joints is obviously higher than that of those filled with 5183 alloy welding wires. In the weld zone, the microhardness value changes a little almost as a constant. Since Er and Zr have noteworthy functions of grain refining [34, 36], the microhardness value of welded joints filled with 5E06 alloy welding wires is higher, especially in the weld center where the microhardness is heightened by roughly 20HV.

Figure 12 exhibits the vertical microhardness values of the weld center of welded joints filled with two different welding materials. The comparison reveals that the microhardness of the weld zone of the two sorts of welded joints change only a little, the discrepancy of hardness in the weld center filled with 5183 alloy welding wire is within 20 HV and the difference of hardness in weld center filled with 5E06 alloy welding wires is less than 10 HV for the reason that uniform welding parameters are applied to stabilize the welding process to the utmost, which guarantees the relative homogeneity of the weld microstructure and properties. The hardness value of the weld zone filled with 5E06 alloy welding wires is higher than that filled with 5183 alloy welding wires. For 5E06 alloys, the grain

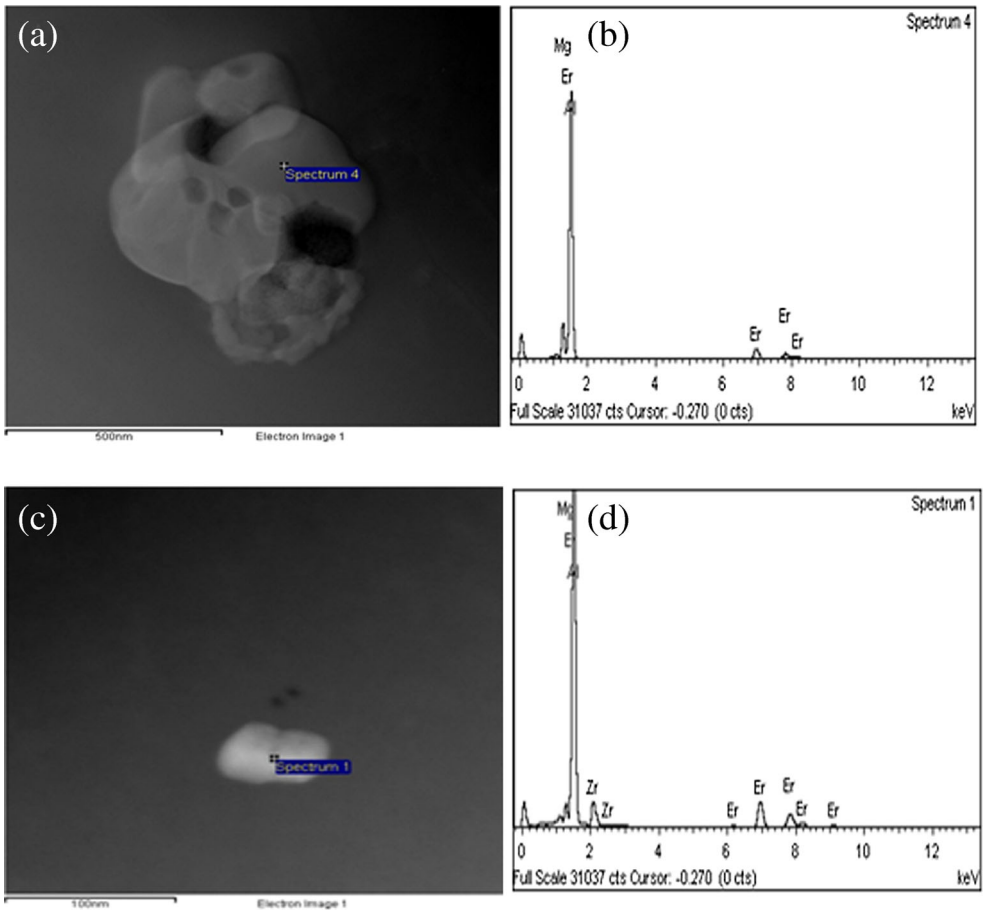

Fig. 10 HAADF STEM image and energy spectrum analysis of the precipitated phase of weld. **a** Morphology of Al3Er. **b** EDS energy spectrum. **c** Morphology of Al3(Er, Zr). **d** EDS energy spectrum

refining effects of Er and Zr tremendously cut down the grain size of weld zone of the joints and the amount of grain boundary correspondingly increases, which will bring more impediments for dislocation transfer, magnifying the resistance to plastic deformation macroscopically displayed in the rise of microhardness and verifying the function of Zr and Er in aluminum alloy in fine grain strengthening [35].

3.2.2 Tensile strength testing

Tensile strength testing for parent metal and welded joints is carried out, respectively. The specimens of welded joints are selected from the conjunctions of welded joints of different passes. Compared with other regions, the microstructures in these conjunctions experience twice thermal cycle where the

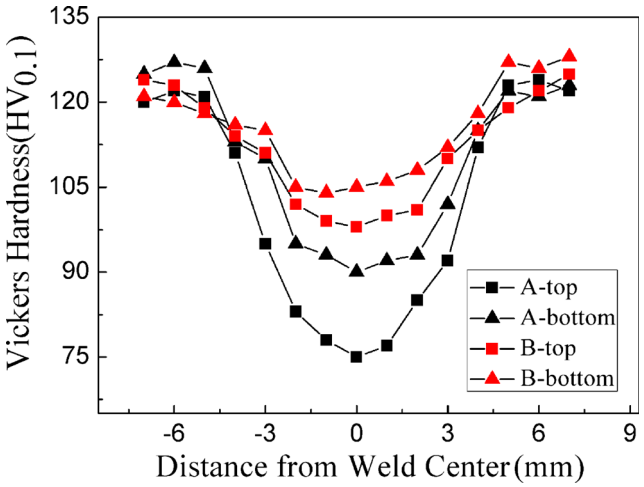

Fig. 11 Horizontal distribution of hardness values of transverse section of welded joints

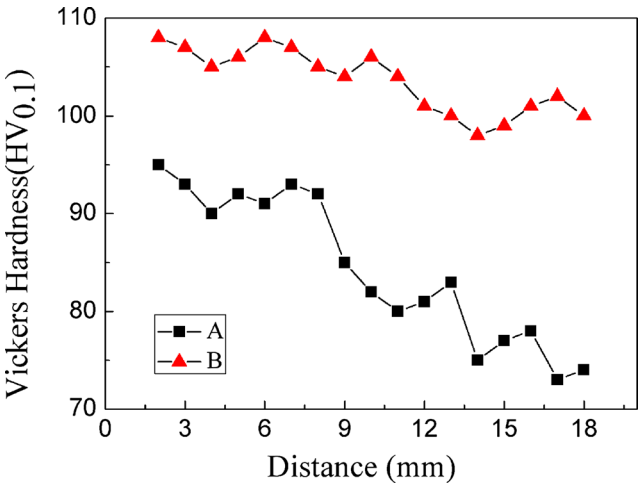

Fig. 12 Vertical distribution of microhardness values of weld center filled with different welding materials

Table 3 Tensile properties of 7A52 base material and welded joints

Specimen	Ultimate tensile strength (Mpa)	Yield strength (Mpa)	Elongation (%)
7A52	468	370	12.5
5183 alloy (between the 1st and the 2nd pass)	290	218	5.4
5183 alloy (between the 2nd and the 3rd pass)	316	225	6.8
5183 alloy (between the 3rd and the 4th pass)	304	210	7.4
5E06 alloy (between the 1st and the 2nd pass)	338	254	8.3
5E06 alloy (between the 2nd and the 3rd pass)	340	265	8.8
5E06 alloy (between the 3rd and the 4th pass)	346	278	9.1

Italic characters are average values

regional organizations change in a more complex manner and the taps become weak easily, better reflecting the mechanical properties of the welded joints in the entirety. In the tensile test, three specimens of welded joints filled with parent metal and different welding materials are taken, respectively. The average values of the joint specimens in the test are given in Table 3, which shows that the strength and tenacity of the welded joints filled with two sorts of welding materials are lower than those of the parent metal. On the one hand, during the welding process, welded joints become as-cast microstructure, and the deformation strengthening effects of aluminum alloy disappear. Meanwhile, some strengthening elements of low boiling points unavoidably evaporate during laser welding, which causes the decline of the mechanical properties of welded joints; on the other hand, the overall mechanical properties applying welding materials are lower than those of parent metal. Debroy T. [39] et al., applying Langmuir theories, explained the mechanism of evaporation loss of the alloying elements and worked out the changes of the element content of 5182 aluminum alloy weld. The parent weld metal and welding wires contain strengthening alloying elements such as Mg and Zn. The fusion point of Mg is similar to that of aluminum, but the boiling point of Mg is lower than that of aluminum. The ER5183 alloy welding wires contain a lot of Mg which plays the role of solution strengthening. The strength of different aluminum rises when the amount of Mg is increased. For this reason, the huge evaporation loss of Mg in the welding process results in the further decline in strength [40].

The fracture of all the welded joints filled with 5183 alloy welding wire occurs to the weld while that of welded joints filled with 5E06 alloy welding wire transits from the fusion zone to HAZ. The mechanical property testing bears witness that welded joints of Zr and Er micro-alloying welding materials boast superior overall mechanical properties, with corresponding tensile strength and yield strength higher than that of 5183 alloy welding wire by 38 and 48 MPa or so, respectively. This is because as Er and Zr are added in Al-Mg-Mn, a large amount of fine Al_3Er and Al_3 (Er, Zr) particles in dispersed distribution are precipitated in the matrix. Such particles are coherent with the matrix and have relatively high thermal stability. On the one hand, Al_3Er and Al_3 (Er, Zr) particles exert intense pinning effects upon the movement of grain boundary, which can impede the movement of grain boundary so as to hinder the growth of grains. Grain refinement can significantly enhance the yield strength of metal. On the other hand, Al_3Er and Al_3 (Er, Zr) particles produce forceful pinning effects upon the mismatching movement so as to increase the strength of the alloy. It can thus be seen that the intensity of the welded joints is improved by grain refinement and strengthening resulting from the addition of Er and Zr as well as the precipitation strengthening of Al_3Er and Al_3 (Er, Zr) particles [35, 36].

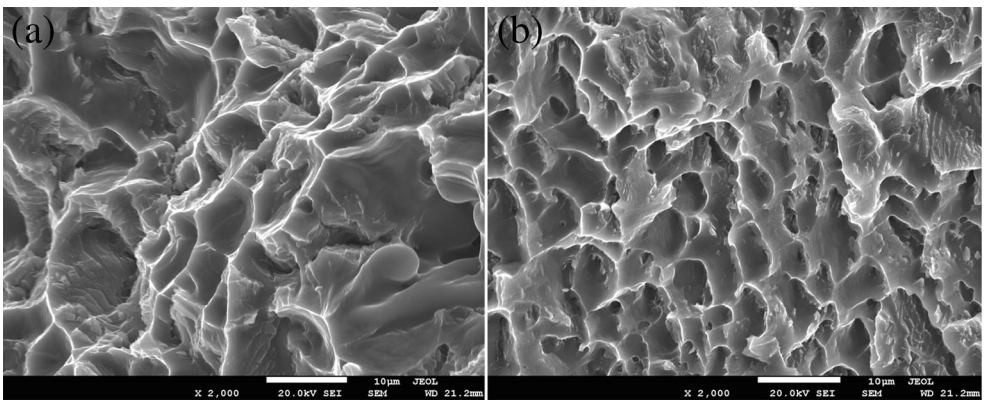

Fig. 13 **a** Morphology of fracture of welded joints filled with 5183 alloy welding wires. **b** Morphology of fracture of welded joints filled with 5E06 alloy welding wires

Figure 13 indicates the typical morphology of the fracture of the welded joints of two distinctive welding materials. The fracture of the welded joints filled with 5183 alloy welding wire displays the features of hybrid cracking with a glide plane of 45°. Comparatively, the dimple of the tensile fracture of the welded joints filled with 5E06 alloy welding wire is finer in size, shallower in depth and in mesh distribution, corresponding to higher strength, lower plasticity and huge quantities of tearing ridges, and a small number of second phase particles on the surface. The primary reason is that the tensile cracking expands in the weld zone, and first, take the second phase of a greater size at the grain boundary or within the grain as the nucleus to form micro-cavern, then after the micro-cavern extends to a certain size, the features of fracture of small dimples around big dimples come into being.

4 Conclusions

This paper studies the 20-mm thick 7A52 aluminum alloy plates reliably welded by means of fiber laser in combination with super narrow gap grooves and compares the microstructure and mechanical properties of the welded joints filled with 5183 alloy welding wires and 5E06 alloy welding wires. In accordance with the experimental results and discussion, the following conclusions are drawn:

(1) By applying pure laser backing weld combined with the technique of laser welding with filler wire, the welding of large and thick aluminum alloy plates by KW laser is realized. The adoption of single U and I grooves is beneficial for the ideal fusion of the base and the side walls. The gap of super narrow groove is no more than 4 mm, which cuts down the weld metal deposition and contribute to the good microstructure and mechanical properties of the welded joints.

(2) Welded joints filled with two diverse welding materials, without macroscopic cavities, inclusion or cracks, can be obtained through the optimized processing parameters. There are two types of HAZs in the super narrow gap welded joints. The first sort is the HAZ near the fusion line while the other is the coarse grain zone generated in the interlayer transition region. In the latter zone, multilayer and single pass welding process is applied, the weld layer is rather thin, the subsequent pass has the effects of thermal treatment upon the preceding pass in stimulation of grain refinement, and the transition region of the interlayer HAZ is extremely narrow.

(3) By applying Al-Mg compound micro-alloying welding wires to weld 7A52 aluminum alloy, the tensile strength, yield strength, and elongation of the welded joints are improved. The observations of the weld zone notice plenty of equiaxed grains of good mechanical properties whose mechanisms include grain refining of Zr and Er compound particles and precipitation strengthening of themselves.

Acknowledgments The paper is financially supported by 973 Project of China, No. 2011CB013403. The authors are grateful to Ling Zhao and Qing Liu for the valuable assistance they have provided with in various aspects of the research program.

References

1. Wu YF, Kim GY, Russell AM (2012) Effects of mechanical alloying on an AL6061-CNT composite fabricated by semi-solid power processing. Mater Sci Eng A 48:164–172
2. Chen CS, Yang JG, Tan AH (2009) Study of welding peak temperatures on microstructures and hardness of heat affected zone in 2024-T3 aluminium alloy. Mater Sci Technol 25:896–904
3. Hu B, Richardson IM (2007) Microstructure and mechanical properties of AA7075(T6) hybrid laser/GMA welds. Mater Sci Eng A 459:94–100
4. Rhodes CG, Mahoney MW, Bingel WH (1997) Effect of friction stir welding on microstructure of 7075 aluminum. Scr Mater 36:69–75
5. Jones MJ, Heurtier P, Desrayaud C (2005) Correlation between microstructure and microhardness in a friction stir welded 2024 aluminium alloy. Scr Mater 52:693–697
6. Sullivan A, Robson JD (2008) Microstructural properties of friction stir welded and post-weld heat-treated 7449 aluminium alloy thick plate. Mater Sci Eng A 478:351–360
7. Cavaliere P, Cerri E, Squillace A (2005) Mechanical response of 2024-7075 aluminium alloys joined by friction stir welding. J Mater Sci 40:3669–3676
8. Amancio-Filho ST, Sheikhi S, Dos-Santos JF, Bolfarini C (2008) Preliminary study on the microstructure and mechanical properties of dissimilar friction stir welds in aircraft aluminium alloys 2024-T351 and 6056-T4. J Mater Process Technol 206:132–142
9. Wei ST, Hao CY, Chen JC (2007) Study of frition stir welding of 1420 aluminum-lithium alloy. Mater Sci Eng A Struct 452:170–177
10. Koteswara SR, Madhusudhana RG, Srinivasa RK (2005) Reasons for superior mechanical and corrosion properties of 2219 aluminum alloy electron beam welds. Mater Charact 40:236–248
11. Zhang C, Li G, Gao M, Yan J, Zeng XY (2013) Microstructure and process characterization of laser-cold metal transfer hybrid welding of AA6061 aluminum alloy. Int J Adv Manuf Technol 68:1253–1260
12. Balasubramanian V, Ravisankar V, Madhusudhan Reddy G (2008) Influences of pulsed current welding and post weld aging treatment on fatigue crack growth behaviour of AA7075 aluminium alloy joints. Int J Fatigue 30:405–416
13. Yu YC, Wang CM, Hu XY (2010) Porosity in fiber laser formation of 5A06 aluminum alloy. J Mech Sci Technol 24:1077–1082
14. Shi H, Zhang K, Xu ZY, Huang TY, Fan LW, Bao WN (2014) Applying statistical models optimize the process of multi-pass narrow-gap laser welding with filler wire. Int J Adv Manuf Technol 75:279–291
15. Yu YC, Yang SL, Yin Y (2013) Multi-pass laser welding of thick plate with filler wire by using a narrow gap joint configuration. J Mech Sci Technol 27:2125–2131
16. Singh V, Prasad KS, Gokhale AA (2004) Effect of minor Sc additions on structure, age hardening and tensile properties of aluminium alloy AA8090 plate. Scr Mater 50:903–908

17. Fuller CB, Krause AR, Dunand DC M (2002) Microstructure and mechanical properties of a 5754 aluminum alloy modified by Sc and Zr additions. Sci Eng A 338:8–16
18. Norman AF, Hyde K, Costello F (2003) Examination of the effect of Sc on 2000 and 7000 series aluminium alloy castings: for improvements in fusion welding. Mater Sci Eng A 354:188–198
19. Halevy OI, Beeri JH (2012) Sc-strengthened commercial purity aluminum under high pressure. Mater Sci 45:589–592
20. Costa S, Puga H, Barbosa J, Pinto MP (2012) The effect of Sc additions on the microstructure and age hardening behaviour of as cast Al-Sc alloys. Mater Des 42:347–352
21. Lefebvre W, Danoix F, Hallem H (2009) Precipitation kinetic of Al3(Sc, Zr) dispersoids in aluminium. J Alloys Compds Compd 470:107–110
22. Xing PF, Gao B, Zhuang YX, Liu KH, Tu GF (2010) On the modification of hypereutectic Al-Si alloys using rear earth Er. Acta Metall Sin 23:327–333
23. Wen SP, Xing ZB, Huang H (2009) The effect of erbium on the microstructure and mechanical properties of Al-Mg-Mn-Zr alloy. Mater Sci Eng A 516:42–49
24. Nie ZR, Li BL, Wang W (2002) Research on rare earth in aluminum. Mater Sci Forum 402:1731–1736
25. Satoh BK, Toyoda M (1975) Joint strength of heavy plates with lower strength weld metal. Weld J 54:311–319
26. Nowak D, Feng G, Jones M, Erikson C (2004) Laser hot-wire welding for minimizing defects. ICALEO
27. Onishi T, Mizutani M, Kawahito Y, Katayama S (2009) High-power fiber laser butt welding of thick high-strength steel plate using sensing system with hot wire. ICALEO
28. Dittrich D, Schedewy R, Brenner B, Standfuß J (2013) Laser-multi-pass-narrow-gap-welding of hot crack sensitive thick aluminum plates. Phys Procedia 41:225–233
29. Chen K, Xiao RS, Zuo TC, Ji Q (2005) Laser welding of Al-Mg alloy with the thin plate. Proc SPIE 5629:155–160
30. Katayama S, Iviizutanf M, Matsunawa A (2003) Development of porosity prevention procedures during laser welding. Proc SPIE 4831:281–288
31. Turnbull D (1950) Formation of crystal nuclei in liquid metals. J Appl Phys 21:1022–1028
32. Witzke S, Riquet JP (1982) Columnar-equiaxed transition in Al-Cu alloy ingots. Acta Metall 30:1717–1722
33. Duggan G, Tong M, Browne DJ (2015) Modelling the creation and destruction of columnar and equiaxed zones during solidification and melting in multi-pass welding of steel. Comput Mater Sci 97: 285–294
34. Li HY, Gao ZH, Yin H, Jiang HF, Su XJ, Bin J (2013) Effects of Er and Zr additions on precipitation and recrystallizaton of pure aluminum. Scr Mater 68:59–62
35. Yang DX, Li XY, He DY, Huang H (2013) Effect of minor Er and Zr on microstructure and mechanical properties of Al–Mg–Mn alloy (5083) welded joints. Mater Sci Eng A 561:226–231
36. Wen SP, Gao KY, Li Y, Huang H, Nie ZR (2013) Effect of gap on plasma and molten pool dynamics during laser lap welding for T-joints. Int J Adv Manuf Technol 69:1105–1112
37. Jandaghi M, Parvin P, Torkamany MJ, Sabbaghzadeh J (2009) Measurement of the composition change in Al5754 alloy during long pulsed Nd:YAG laser welding based on LIBS. J Phys D Appl Phys 42:205301.1–205301.8
38. Lefebvre F, Ganguly S, Sinclair I (2005) Micromechanical aspects of fatigue in a MIG welded aluminium airframe alloy. Mater Sci Eng A 397:338–345
39. Zhao H, Debroy T (2001) Weld metal composition Chang during conduction mode laser welding of aluminum alloy 5182. Metall Mater Trans B 32:163–172
40. Dilthey U, Goumeniouk A, Lopota V (2001) Development of a theory for alloying element losses during laser beam welding. J Phys D Appl Phys 34:81–86